Enhancing Electrochemical CO₂ Reduction Activity of Polymer-Encapsulated Cobalt Phthalocyanine Films by Modulating the Loading of Catalysts, Polymers, and Carbon Supports

Taylor L. Soucy $^{\dagger,\#}$, Yingshuo Liu $^{\dagger,\#}$, Jonah B. Eisenberg † , Charles C. L. McCrory †,§,*

[†]Department of Chemistry, University of Michigan, 930 N University Ave, Ann Arbor Michigan, 48109-1055, United States.

§Macromolecular Science and Engineering Program, University of Michigan, Ann Arbor, Michigan, 48109-1055, United States.

*T.L.S and Y.L. contributed equally.

ABSTRACT

Cobalt phthalocyanine (CoPc) has been extensively studied as a catalyst for the electrochemical reduction of CO₂ to value-added products. Previous studies have shown that CoPc is a competent and efficient catalyst when immobilized onto carbon-based electrodes using a polymer binder, especially when immobilized with a graphitic carbon powder support to increase charge transport. In this study, we systematically explore the influence of incorporating graphite powder (GP) into a polymer-encapsulated CoPc on the system's activity for the electrochemical reduction of CO₂.

We report a protocol for incorporating GP into CoPc/polymer/GP catalyst films that facilitates physisorption of CoPc to GP, leading to increased activity for CO₂ reduction. We show that the activity for CO₂ reduction increases with GP loading at low GP loadings, but at sufficiently high GP loadings the activity plateaus as charge transfer is sufficiently fast to no longer be rate limiting. We also demonstrate that axial coordination is still important even in the presence of GP, suggesting that CoPc does not fully coordinate to heteroatoms on the GP surface. We develop a set of optimized conditions under which the CoPc/polymer/GP catalyst systems reduce CO₂ with higher activity and similar selectivity to previously reported CoPc/polymer films on edge-plane graphite electrodes. The procedures outlined in this study will be used in future studies to optimize catalyst, polymer, and carbon support loadings for other polymer-catalyst composite systems for electrocatalytic transformations.

INTRODUCTION

There has been intense recent interest in cobalt phthalocyanine (CoPc) as an active and efficient electrocatalyst for the CO₂ reduction reaction (CO₂RR).¹⁻⁴⁴ Recent studies have shown that CoPc is even capable of reducing CO₂ to methanol via a cascade (or domino) catalysis mechanism involving a CO intermediate when CoPc is adsorbed onto carbon nanotubes (CNTs) and studied under specific conditions.^{19,29,33,45,46} Our interest in CoPc has focused on using the system as a model for understanding the parameters that influence the electrocatalytic activity of polymerencapsulated molecular catalysts and related membrane-coated electrocatalyst systems.⁴⁷ In particular, our work and that of others has shown that incorporating CoPc within a poly-4-vinylpyridine (P4VP) polymer results in increased activity and reaction selectivity for the CO₂RR to CO over the competitive hydrogen evolution reaction (HER) in pH 5 phosphate electrolytes

(Figure 1a).^{3,5,13} By using a combination of systematic modifications of the polymer-catalyst composite system,^{13,24} kinetic isotope effect and proton inventory studies,²⁴ and *in situ* electrochemical X-ray absorbance spectroscopy measurements,³⁶ we have shown that both the coordination environment and chemical microenvironment surrounding the CoPc active sites play a crucial role in modulating the activity and selectivity of the CoPc-P4VP composite materials (Figure 1a).

In our previous studies, we avoided the use of conductive carbon powder supports commonly used to enhance charge transport because these carbon powders can influence the nature of the polymer-catalyst interactions. For example, carbon powders with large concentrations of heteroatoms such as doped graphene and graphene oxide can facilitate interactions between the CoPc and the S, N, or O heteroatoms on the carbon surface, thus influencing the catalytic mechanism.^{27,48,49} Moreover, planar metal phthalocyanines and related complexes strongly physisorb to graphitic carbon surfaces due to π - π interactions between the conjugated graphitic surfaces and the aromatic Pc ring which affects the electronic structure of the system, as shown in several CoPc-CNT X-ray absorption studies. 8,14,50-54 Therefore, increasing the surface area of graphitic carbon through the incorporation of carbon powders may alter the electronic and chemical microenvironment surrounding the CoPc and complicate mechanistic understanding while increasing overall activity.⁵⁵ While our choice to avoid using conductive carbon-powder supports enabled us to better study the influence of polymer encapsulation on catalytic mechanisms, it likely limited the overall activity of our catalyst-polymer system due to inefficient charge transport. 47,56,57

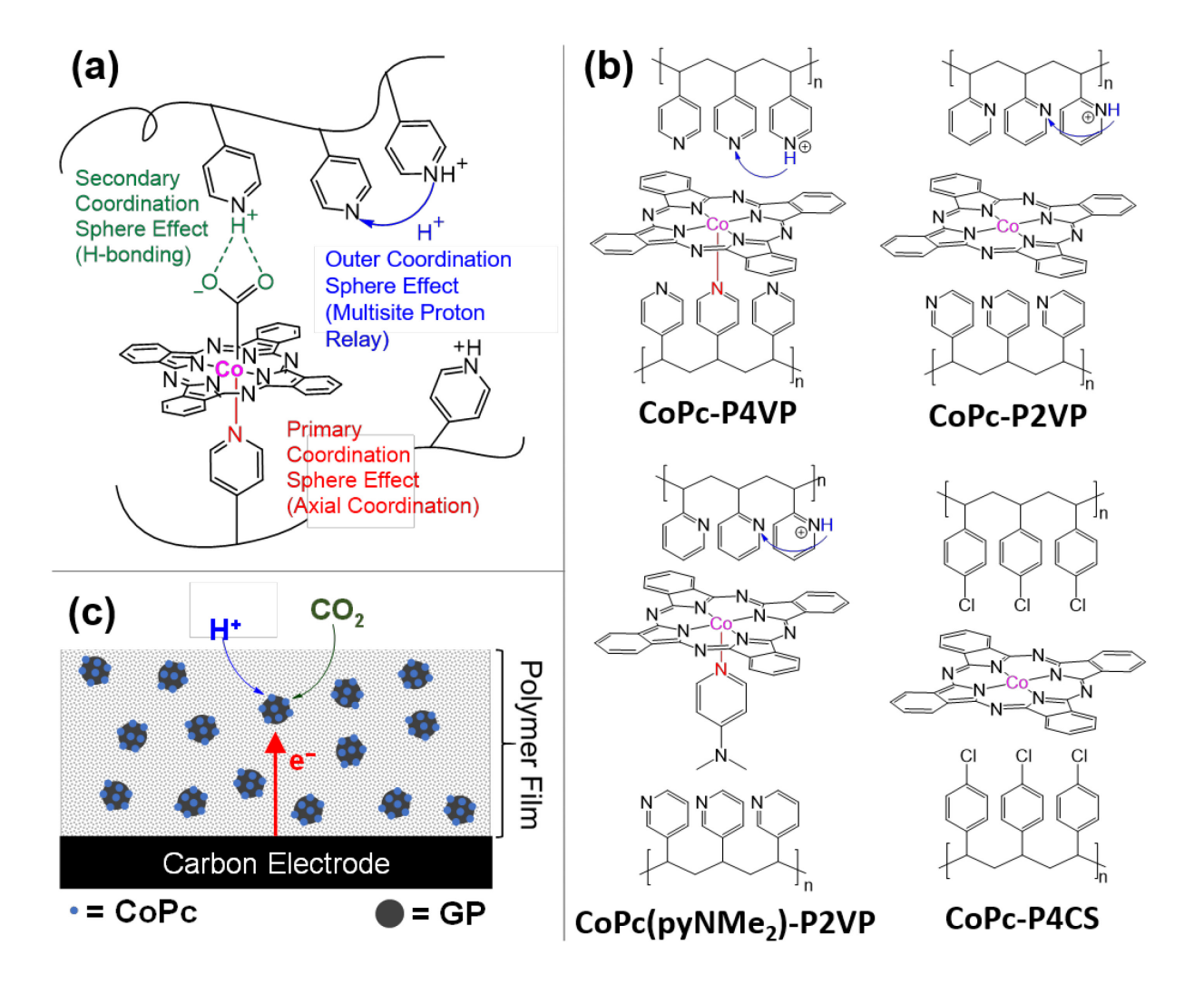


Figure 1. (a) Encapsulating cobalt phthalocyanine (CoPc) within the coordinating polymer poly-4-vinylpyridine (P4VP) results in a composite CoPc-P4VP system that shows enhanced activity for the CO₂ reduction reaction compared to the parent CoPc system. The increased activity is attributed to primary, secondary, and outer-coordination sphere effects imbued by the P4VP polymer on the CoPc catalyst active site. Adapted from Ref. 36 with permission from The Royal Society of Chemistry. (b) Polymer-catalyst composite systems investigated in this work along with their postulated coordination environments and proton relays. (c) A schematic illustration of CoPc immobilized onto a graphite-powder support and encapsulated within a polymer film composed of the various polymers show in (b).

In a few studies, researchers have incorporated graphitic carbon into CoPc films with the purpose to improve charge transport (see Supplementary Table S1). For example, in one study, a 10-fold increase in activity was observed when Vulcan XC-72 and CNTs were incorporated into a CoPc catalyst deposition solution.³³ In another study, major activity differences were observed in CoPc-based gas-fed electrolyzers that incorporated different carbon sources (carbon fibers, graphite, Vulcan XC-72, and activated carbon).⁴⁶ However, there are few studies with experiments to explicitly explore the impacts of charge and substrate transport on the CO₂RR by CoPc-polymer composite catalysts. Such studies are crucial because, as demonstrated in this report, activity metrics can vary significantly despite very similar preparation methods.

Based on these previous uses of carbon supports in CoPc systems for the CO₂RR, we believe there is significant space to improve the overall activity of the CoPc-P4VP system through the incorporation of carbon powder supports. However, care must be taken to understand how the impact of incorporating this graphitic support influences the selectivity and activity of the CO₂RR. Understanding of the effects of incorporating carbon supports us particularly important in developing gas-fed flow electrolyzer systems incorporating molecular catalyst such as CoPc. ^{25,58}

In this study, we directly add graphite powder (GP) as a carbon support to CoPc/polymer electrocatalyst to increase charge transport within the resulting polymer films (Figure 1b). We show that incorporating GP within the CoPc-P4VP system deposited onto a glassy carbon electrode leads to a CoPc-P4VP/GP/GCE composite material that operates with the similar reaction selectivity but significantly increased activity for the CO₂RR compared to CoPc-P4VP without incorporated GP deposited onto glassy carbon (CoPc-P4VP/GCE) and edge-plane graphite electrodes (CoPc-P4VP/EPG).

We postulate that observed increases to catalytic activity are because GP incorporation into the film facilitates electron transport to the exterior catalytic sites, which increases the total number of sites within the film that are active for the CO₂RR and decreases the average distance substrate must transport through the film to reach an electroactive CoPc catalyst molecule.¹¹ To test this postulate, we explored how different loadings and ratios of CoPc and GP influenced the catalytic activity of the system. For example, we show that at sufficiently high loading of CoPc in the CoPc-P4VP/GP/GCE system, further increasing the loading of CoPc has no appreciable effect on activity—there is a plateau in activity as CoPc loading is increased. We also show that increasing the CoPc-P4VP loading while keeping the GP loading constant leads to a decrease in overall activity, but that increasing the CoPc-P4VP loading with added GP (increasing GP loading along with CoPc and P4VP) results in an increase in overall activity at a smaller CoPc loading, before eventually reaching a plateau where increasing CoPc-P4VP and GP loading no longer influences activity. These observed activity plateaus suggest that at sufficiently high CoPc, P4VP, and GP loading, another effect limits the activity. This other effect may be inefficient CO₂ or H⁺ transport, CoPc aggregation, or a combination of these effects. 18,21

In addition, we show that axial coordination to the CoPc by the polymer in CoPc-P4VP/GP or an added ligand in CoPc(pyNMe₂)-P2VP/GP is necessary to achieve the highest maximum activity. This result suggests that although we cannot exclude the possibility that functional groups on the GP coordinate to CoPc in the composite system, axial coordination to a pyridyl or pyNMe₂ residue is still important for catalytic activity and outcompetes any coordination to functional groups on the carbon surface.

Through these systematic studies of the effect of catalyst, polymer, and graphite powder loading on catalyst activity for the CO₂RR by CoPc-P4VP/GP/GCE, we elucidate the relative

importance of charge and substrate transport on catalytic activity. We demonstrate that optimizing catalyst/polymer systems for activity and selectivity requires careful consideration of both the loading and preparation of the catalyst/polymer composite materials and carbon supports.

EXPERIMENTAL

Materials

All purchased chemicals were used as received unless otherwise specified. All water used in this study was ultrapure water (18.2M Ω cm resistivity), purified with a Thermo Scientific GenPure UV-TOC/UF x CAD-plus water purification system. Carbon dioxide (CO₂, 99.8%) was purchased from Cryogenic Gases and was used as received. Nitrogen (N₂) was boil-off gas from a liquid nitrogen source and was used without further purification. Cobalt phthalocyanine (CoPc, 97%), poly-4-vinylpyridine (P4VP, average Mw ~ 160,000), poly-2-vinylpyridine (P2VP, average Mw ~ 159,000), poly-4-chlorostyrene (P4CS, average Mw ~ 75,000), N,N-Dimethylformamide (DMF, ACS grade), ferrocene carboxylic acid (97%), sodium phosphate monobasic (BioXtra, >99.0%), 4-dimethylaminopyridine (pyNMe₂, \geq 99%), graphite powder (GP, synthetic 20 μ m) and Nafion-117 cation exchange membrane (Nafion) were purchased from Sigma Aldrich and used as received. Sodium hydroxide (NaOH, TraceMetal grade) was obtained from Fisher Scientific. Nitric acid (TraceMetal grade, 67-70%) was purchased from Fisher Scientific. Cobalt ICP standard (1000 ppm in 3% HNO₃) was purchased from Ricca Chemical Company.

Electrolyte Solution Preparation and pH Measurements

All electrolyte solutions were prepared using ultrapure water. All experiments were performed in phosphate solutions of 0.1 M NaH₂PO₄ adjusted to pH 5 by the addition of 1 M NaOH. Prior

to each experiment, the working chamber was sparged with the appropriate gas by using a section of Tygon tubing for at least 30 minutes. The pH after sparging with CO_2 was 4.7. The electrolyte pH before-and-after CO_2 sparging was confirmed using a Fisher Scientific Accumet AB200 pH meter with an Atlas Scientific pH probe electrode calibrated with a three-point calibration curve at pH = 4.01, 7.00, and 10.01.

Preparation of Catalyst Preparation Suspensions

The specified concentrations of the CoPc, polymer, and graphite powder in the preparation suspensions (along with the corresponding CoPc and polymer loading determined by ICP-MS and gravimetric analysis, respectively) are listed in Supplementary Tables S2 – S17 and S19.

CoPc-polymer deposition inks without GP were prepared using the following procedure: a 0.2 mM solution of CoPc dispersed in DMF was prepared via sonication of 0.0058 g of CoPc in 50 mL of DMF for 1 hour in an aluminum foil-jacketed polypropylene conical centrifuge tube (BasixTM). The 0.2 mM solution was then diluted to the desired concentration via the addition of the stock solution to DMF, and the corresponding polymer was added to the diluted CoPc solution.

CoPc-polymer/GP preparation suspensions were prepared via sonication of 0.0052 g of CoPc in 45 mL of DMF for 1 hour in an aluminum foil-jacketed polypropylene conical centrifuge tube (BasixTM). The 0.2 mM CoPc/DMF solution was then diluted to 1 mL of the desired concentration via the addition of the stock solution to DMF in a 20 mL glass scintillation vial. A given mass of polymer was then added to the 20 mL scintillation vial that contained the 1 mL of CoPc/DMF in order to form the desired CoPc-polymer solution. The CoPc-polymer solution was sonicated for 30 minutes to ensure dispersion of the polymer. A given mass of graphite powder was then added to the CoPc-polymer solution to form the CoPc-polymer/GP preparation suspension. Polymer and

graphite powder concentrations are denoted w/v %, meaning 0.01 g GP in 1 mL of CoPc/DMF solution is denoted as 1% GP. Note: graphite powder particles with a diameter of < 20 μ m was used in this study—films made with larger graphite powder particles (diameter \sim 100 μ m) led to visible delamination during the electrochemical measurements.

CoPc(pyNMe₂)-P2VP/GP preparation suspensions were prepared via sonication of 0.00518 g of CoPc and 1.0995 g of 4-Dimethylaminopyridine in 45 mL of DMF for 1 hour in an aluminum foil-jacketed polypropylene conical centrifuge tube (BasixTM) to form a 0.2 mM CoPc / 0.2 M pyNMe₂ / DMF solution, ensuring 5-coordinate character by using 1000:1 pyNMe₂:CoPc ratio, as we have done previously.⁴⁴ This solution was then diluted to 1 mL of the desired CoPc and pyNMe₂ concentration via the addition of the stock solution to DMF in a 20 mL scintillation vial. A given mass of P2VP was then added to the 20 mL scintillation vial that contained the 1 mL of CoPc/DMF in order to form the desired CoPc(pyNMe₂)-P2VP solution, which was then sonicated for 30 minutes to ensure the dispersion of P2VP. A mass of 0.01 g of graphite powder was then added to the CoPc(pyNMe₂)-P2VP solution and was sonicated for 30 minutes to ensure the dispersion of graphite powder.

Preparation of Deposition Inks

After the addition of GP, the CoPc-polymer/GP or CoPc(pyNMe₂)-P2VP/GP preparation suspensions were sonicated for 30 min to ensure dispersion of the GP. A Teflon stir bar was added to the scintillation vial, and the preparation suspension was stirred for 12 h at 500 rpm. The preparation suspension was then centrifuged at 14,000 rpm for 30 minutes at -11°C in an Eppendorf 5430R refrigerated centrifuge. The DMF was decanted, and 1 mL of fresh DMF was added to the

remaining pellet. The remaining graphitic pellet suspended in fresh DMF (denoted as the deposition ink) was vortexed for 30 sec at 3000 rpm, and sonicated for 30 sec.

The catalyst loading in the deposition inks were determined by digesting the graphitic pellet after the centrifugation step and measuring the metal content using inductively coupled plasmamass spectrometry (ICP-MS, PerkinElmer Nexion 2000). A volume of 15 mL of 1 M TraceMetal Grade HNO₃ was added to the graphitic pellet, and the resulting graphite/nitric acid slurry was stirred overnight. The slurry was then filtered using a cellulose syringe (0.45 μm, Titan 3 regenerated cellulose, Fisher Scientific) to remove graphite powder and polymer. The cobalt concentration of the resulting solution was then measured using ICP-MS, calibrated using Co calibration standards in 1 M HNO₃ at 10, 50, 100, and 500 ppb, and standard at 0 ppb along with internal standard of Bismuth. The conversion between the calculated ppb to molar CoPc loading in the deposition ink is shown in Equations 1-3:

$$X \text{ ppb } \times \frac{\frac{1 \mu g}{L}}{1 \text{ ppb}} \times 0.015 \text{ L} = \text{mass Co in } \mu g$$
 (1)

mass in
$$\mu$$
g x $\frac{1 \text{ mol Co}}{58.93 \text{ g Co}} \times \frac{10^{-6} \text{ g}}{1 \mu\text{g}} = \text{mol CoPc}$ (2)

$$\frac{\text{mol CoPc}}{\text{0.0010 L initial deposition ink}} = M \text{ CoPc in deposition ink}$$
 (3)

The loading of CoPc for each deposition ink was determined via ICP-MS measurements in at least 3 independently prepared samples, and the average values are reported in Tables S1-S19 along with standard deviations.

The polymer loading in each deposition ink was determined by estimating the mass of polymer removed from the preparation solution during the centrifugation step. After the supernatant is

decanted from the graphite pellet left after centrifugation of the preparation solution, the solvent was evaporated from the supernatant and the mass of the resulting residue (m_{residue}) was measured. The mass loading of polymer in the catalyst deposition ink ($m_{\text{polymer in ink}}$) was estimated by subtracting the mass of catalyst left over in the supernatant ($m_{\text{CoPc in supernatant}}$) from the total mass of the residue (m_{residue}) as shown in Equations 4-6.

$$m_{\text{CoPc in prep solution}} - m_{\text{CoPc in deposition ink}} = m_{\text{CoPc in supernatant}}$$
 (4)

 $m_{\text{residue}} - m_{\text{CoPc in supernatant}} = m_{\text{polymer in supernatant}}$ (5)

 $m_{\text{polymer in preparation suspension}} - m_{\text{CoPc in supernatant}} = m_{\text{polymer in deposition ink}}$ (6)

 $\frac{m_{\text{polymer in deposition ink}}}{1.0 \text{ mL}} = \text{polymer loading}$ (7)

Preparation of Modified Electrodes

5 mm diameter glassy carbon disk electrodes (GCEs) (4 mm thick, 0.196 cm² surface area, Sigradur G, HTW Hochtemperatur-Werkstoffe GmbH) or 5 mm edge plane graphite (EPG) disk electrodes (3.81 mm EPG disk encapsulated in epoxy, 0.114 cm² effective surface area, Pine Research Instrumentation) were used as working electrodes. The GC disk electrodes were polished using a Struers LaboPol-5 polisher with a LaboForce-1 specimen mover. The GC disks electrodes were loaded into a custom-designed brass electrode holder held by the specimen mover with ~5 psi of applied pressure per disk. The GC disk electrodes were sequentially polished with diamond abrasive slurries (DiaDuo-2, Struers) in an order of 9 μm, 6 μm, 3 μm, and 1 μm diameter particle slurries for 1 minute each on synthetic nap polishing pads (MD Floc, Stuers). During polishing, the platen speed was held at 200 rpm, and the head speed at 8 rpm in the opposite rotation from the platen. Between each polishing step, the GC disks were rinsed with water. After the final polishing step, the GC disks were sonicated sequentially in isopropyl alcohol for 3

minutes, ultrapure water for 3 minutes, and 1 M HNO₃ for 30 minutes. The GC disk electrodes were then rinsed with ultrapure water and dried under an N₂ stream. EPG electrodes were polished manually on 600 grit silicon carbide polishing paper (Buehler, CarbiMet) followed by sonication in ultrapure water for ~1 minute and drying under an N₂ stream.

The addition of catalyst deposition ink to the GCE or EPG took place via the following procedure: CoPc-polymer solution was coated on the electrodes via dropcasting 5 μL of solution, allowing the surface to dry in an oven at 60°C for 10 minutes, and then applying a second coating of 5 μL of the solution and drying at the same temperature. For the experiment where the CoPc:P4VP:GP loading was held constant , the CoPc loading was increased by preparing a preparation slurry with 0.0125 mM CoPc and 0.75% P4VP, along with 1%, 0.5%, or 0.1% GP. The resultant CoPc concentrations in deposition inks are reported in Supplementary Tables S8, S10, and S12, respectively. To increase the concentration of CoPc, P4VP, and GP, the deposition ink was dropcasted in 10 μL layers, with each increase in Co and GP being proportional to the addition of another 10 μL deposition. The number of 10 μL layers and the resulting electrode CoPc and GP loadings for this study can be found in Supplementary Tables S9, S11, and S13.

All calculated CoPc, polymer, and GP electrode loadings are organized by figure, and can be found in Supplementary Tables S1-S17 and S19.

Electrochemical Measurements

Electrochemical measurements were conducted using a Bio-Logic SP200 potentiostat/galvanostat, and data were recorded using the Bio-Logic EC-Lab software package. Reference electrodes were commercial saturated calomel electrode (SCE), externally referenced to ferrocenecarboxylic acid in 0.2 M phosphate buffer at pH 7 (0.284 V vs. SCE), and auxiliary

electrodes were carbon rods (99.999%, Strem Chemicals Inc.). Working electrodes were the CoPc-polymer/GP-, CoPc(L)-polymer/GP-, or CoPc-polymer-modified GCEs or the CoPc-polymer EPGs. In all cases, the working electrode was separated from the auxiliary electrode by a Nafion membrane. Unless otherwise noted, all electrochemical measurements were conducted at least three times with independently prepared electrodes, all values reported are the average of these repetitions, and all reported errors are standard deviations. Data were recorded using the Bio-Logic EC-Lab software package.

For rotating disk electrode chronoamperomentric step (RDE-CA) measurements, the modified GCE working compartment was assembled using a Pine Research Instrumentation E6-series change disk rotating disk electrode (RDE) assembly attached to an MSR rotator. RDE-CA measurements were conducted at 1600 rpm with 2-minute potential steps at every 0.05 V from -1.00 to -1.25 V vs. SCE. The 1600 rpm rotation rate was used to ensure steady-state substrate delivery to the electrode surface in a way that is not present in a longer controlled potential electrolysis (CPE) experiment. RDE-CA measurements were conducted in a custom twocompartment glass cell. In the first compartment, the working electrode with GCE assembly was suspended in 30 mL buffer solution with 3 gas inlets and one inlet for the reference electrode. The second compartment contained ~15 mL solution with the auxiliary electrode. The compartments were separated by a Nafion membrane. Both compartments were sparged with N₂ or CO₂ for ~30 minutes prior to each set of measurements, and the headspace was blanketed with CO₂ during the measurements. The CO₂ used for these electrochemical experiments was first saturated with electrolyte solution by bubbling through a gas washing bottle filled with water, to minimize electrolyte evaporation in the cell throughout the course of the measurements. iR drop was measured prior to the experiment and was compensated at 85% via a positive feedback loop from the software. In general, our electrochemical cell for CA measurement had Ru $\sim \! 150~\Omega$ in all electrolyte solutions.

Controlled potential electrolysis (CPE) experiments were conducted at room temperature in custom, gas-tight, two-chamber U-cells as previously reported. The modified working electrode was held in an RDE internal hardware kit (Pine Research Instrumentation) and mounted into a custom PEEK sleeve. For the electrolysis measurements, the main chamber held the working electrode and an SCE reference electrode in ~25 mL electrolyte, and the headspace was measured after each experiment by measuring the amount of water needed to refill the main chamber. The auxiliary chamber held the auxiliary carbon rod electrode in 15 mL electrolyte. The two chambers were separated by Nafion cation exchange membrane. Prior to each experiment, both chambers were sparged with CO_2 for ~30 min and then the main chamber was sealed under CO_2 atmosphere. The uncompensated resistance of the cell was measured with a single-point high-frequency impedance measurement. The CPE measurements were not compensated for iR drop, and the potential value reported is the real applied potential. In general, our electrochemical cell for CPE had $Ru = ~300 \ \Omega$. Product distribution for controlled potential electrolysis results can be found in Supplementary Table S31.

Product Detection and Quantification

After CPE, gaseous and liquid samples were collected and analyzed using gas chromatography (GC). For gaseous samples, analysis was conducted using a Thermo Scientific Trace 1310 GC system with two separate analyzer channels for the detection of H₂ and C1-C2 products. A Pressure-Lok gas-tight syringe (10 mL, Valco VICI Precision Sampling, Inc.) was used to collect 5 mL aliquots from the main chamber headspace of the cell, and each aliquot was injected directly

into the 3 mL sample loop. Using a custom valve system, column configuration, and method provided by Thermo Scientific, gases were separated such that H_2 was detected on the first channel using an Ar carrier gas and thermal conductivity detector (TCD) and all other gases were detected on the second channel using a He carrier gas and a TCD. The GC system was calibrated using calibration gas mixtures (SCOTTY Specialty Gas) at $H_2 = 0.01$, 0.02, 0.05, 0.5, and 1% v/v and CO = 0.02, 0.05, 0.5, 1, and 7% v/v. Chromatographs were analyzed by using the Chromeleon Console WorkStation software.

Faradaic efficiencies of gaseous products were calculated via Equation 8:

$$FE = \frac{\frac{V_{HS}}{V_g} \times G \times n \times F}{O}$$
 (8)

where V_{HS} is the headspace volume in mL of the working chamber, V_g is the molar volume of gas at 25°C and 1.0 atm (24500 mL/mol), G is the volume percent of gaseous product determined by GC (%), n is the number of electrons required for each product (n = 2 for H₂ and CO), F is the Faraday constant (C/mol) and Q is the charge passed in Coulombs.

RESULTS AND DISCUSSION

In our prior work in this area, we immobilized CoPc-P4VP and related systems onto edgeplane graphite (EPG) electrodes to form CoPc-P4VP/EPG materials. ^{13,36,44,47} In these studies, we sought to understand the microenvironment surrounding the polymer-encapsulated CoPc site. EPGs were an optimal choice of electrode because the high surface area of the electrode surface and intercalation of the CoPc catalyst between the graphitic sheets facilitated charge transport to the CoPc active sites. In this study, to understand better the role of the graphite powder support (GP) on activity, we immobilized polymer/catalyst composite system onto planar glassy carbon electrodes (GCEs) and measured the activity of multiple samples with varying levels of CoPc loading (Figure 2a). Planar GCEs are smoother than EPG electrodes and do not have aligned graphite sheets that allow for intercalation; they are therefore an appropriate electrode material for studying the effect of graphite powder incorporation on charge transport. Activity is reported as the absolute value of the catalytic current density measured in CO₂-saturated phosphate solutions at pH 5.

CoPc-P4VP films incorporating graphite powder on the GCE electrodes (CoPc-P4VP/GP/GCE) have more than double the activity compared to CoPc-P4VP/GCE without graphite powder at any given catalyst and polymer loading (Figure 2a). CoPc-P4VP/GCE not only reduces CO₂ with less activity than CoPc-P4VP/GP/GCE, but also with significantly less activity than CoPc-P4VP films on edge-plane graphite (CoPc-P4VP/EPG). We postulate that the small magnitude current densities for CoPc-P4VP/GCE compared to CoPc-P4VP/EPG and CoPc-P4VP/GP/GCE is due to poor charge transport through the polymer film on the GCE surface. SEM images for CoPc-P4VP/GP/GCE (Figure 2b) show that GP incorporation into the film leads to high surface area features that enhance charge transport throughout the polymer film. SEM images of CoPc-P4VP/EPG (Figure 2c) show similar high-surface area carbon features with slightly more rigid parallel packing due to the EPG electrode structure. CoPc-P4VP/GCE with no carbon support is relatively featureless aside from slight pitting due to polishing methods (Figure 2d). The lack of high-surface area carbon features in CoPc-P4VP/GCE make it more difficult for charge to transport from the smooth electrode surface to CoPc molecules at the exterior of the film compared to CoPc-P4VP/EPG and CoPc-P4VP/GP/GCE.

Note that the increased activity with added GP for the CoPc-P4VP/GP/GCE system only occurs when the films are prepared as described in the experimental section with centrifugation. Simply mixing the GP into a CoPc-P4VP ink with no centrifugation step results in films that have

markedly lower activity for the CO₂RR (Figure S1). The centrifugation step concentrates the CoPc-P4VP system near the GP and likely facilitates physisorption to the particles, which in turn promotes efficient charge transport to the CoPc.^{33,59,60} Note that most other reported methods for preparing CoPc films with carbon supports do not include this centrifugation step, which could be one reason for such large differences in the reported performance of these systems.

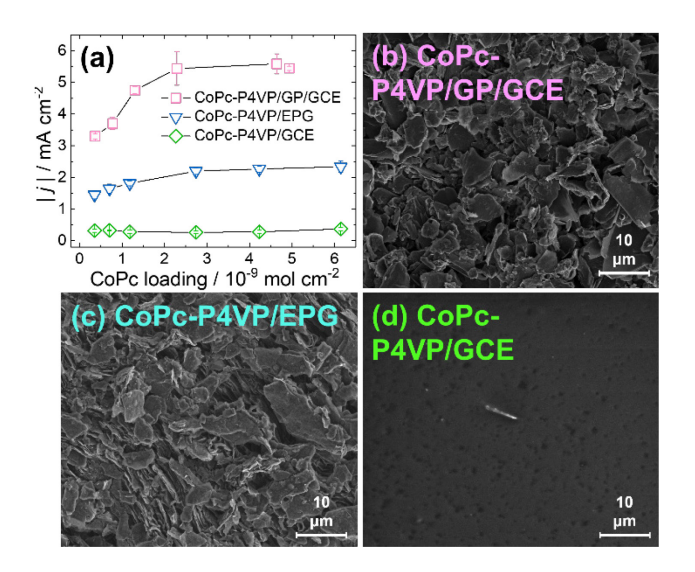


Figure 2. (a) A plot of the absolute value of the average current density from RDE-CA measurements at −1.25 V vs SCE in CO₂-saturated 0.1 M phosphate solution at pH 5 reported as a function of CoPc loading for CoPc-P4VP/GP/GCE (10 mg/mL GP), CoPc-P4VP/EPG, and CoPc-P4VP/GCE. Each film has the same P4VP loading. All data points are reported as averages from at least three experiments on independently prepared samples, and the error bars represent standard deviations. The solid black lines connecting the points are guides to the eye, and not indicative of fits of the data. The loadings of CoPc, P4VP, and GP for each data point is summarized in Supplementary Table S2-4, representative RDE-CAs for selected CoPc loadings are shown in Supplementary Figure S2 and S4-S5, and activity data is summarized in Supplementary Tables S20-21. (b)-(d) SEM images of the catalyst-modified electrodes (b) CoPc-P4VP/GP/GCE (c) CoPc-P4VP/EPG and (d) CoPc-P4VP/GCE.

To determine how modulating the CoPc and GP loading within the CoPc-P4VP/GP/GCE affects the CO₂RR activity, we systematically changed the amount of CoPc and GP in the catalyst deposition inks while maintaining constant CoPc:P4VP ratios. The specific concentrations of CoPc, P4VP, and GP in the deposition inks investigated and the measured loadings on the resulting CoPc-P4VP/GP/GCE electrodes are summarized in Supplementary Tables S2 and S4-S6. A plot of catalytic activity as a function of CoPc loading at different GP loadings is shown in Figure 3a. Another way to visualize this data is by dividing the catalytic activity by the CoPc loading, resulting in a per-CoPc activity metric j_{CoPc} . A plot of j_{CoPc} as a function of CoPc loadings at different GP loadings is shown in Figure 3b.

When no GP is present in the film (0 mg cm⁻² GP loading), the measured CO₂RR activity is relatively constant with increasing CoPc loading (Figure 3a) and there is a corresponding decrease in the normalized activity per CoPc with increasing CoPc loading (Figure 3b). We interpret this result to mean that only a small, constant amount of CoPc near the electrode surface is active as the film loading increases due to inefficient charge transfer to exterior CoPc sites far from the surface in the film.

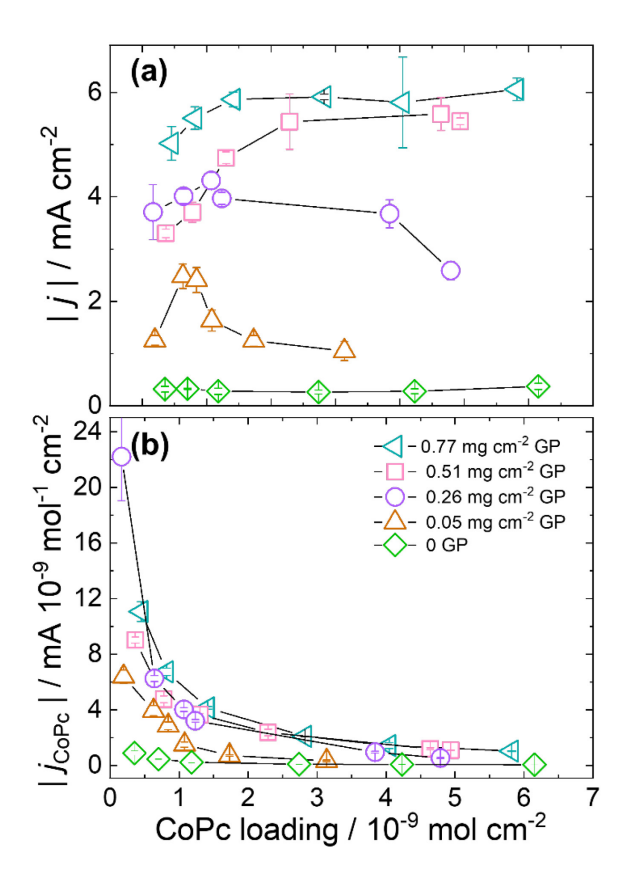


Figure 3. (a) A plot of the absolute value of the average total current density from RDE-CA measurements at -1.25 V vs SCE in CO₂-saturated 0.1 M phosphate solution at pH 5 reported as a function of CoPc loading for CoPc-P4VP/GP/GCE at different GP loadings. For each set of measurements at a given GP loading, the CoPc:P4VP ratio stays constant as CoPc increases. (b) The same data as in (a), but normalized for CoPc loading. The resulting total charge density normalized for CoPc loading, j_{CoPc} decreases as CoPc loading increases. All data points are reported as averages from at least three experiments on independently prepared samples, and the error bars represent standard deviations. The solid black lines connecting the points are guides to the eye, and not indicative of fits of the data. For all measurements, the loading of CoPc, P4VP, and GP for each data point is summarized in Supplementary Table S2-S3 and S5-S7, representative RDE-CAs for selected CoPc loadings are shown in Supplementary Figure S2 and S5S8, and activity data is summarized in Supplementary Tables S20-S24.

For CoPc-P4VP/GP/GCE films with low GP loadings of = 0.05 mg cm⁻², there is an initial increase in the overall activity as the CoPc loading increases, followed by a sharp decrease at higher CoPc loadings (Figure 3a). We interpret these results to suggest that the addition of moderate amounts of GP to the film increases the effective distance in which efficient charge transfer occurs and thus increases activity. However, as the film loading increases with higher CoPc loading at constant CoPc:P4VP ratios, the average film thickness of the resulting CoPc-P4VP/GP/GCE films also increases. The net result is that the individual GP particles are spaced further apart in these thicker films at higher film loadings, inhibiting efficient charge transport to the exterior CoPc. This leads to decreased activity at higher CoPc loadings for these films with relatively moderate or low GP loadings.

At sufficiently high GP loadings ≥ 0.51 mg cm⁻², the activity of the CoPc-P4VP/GP/GCE system increases as the CoPc loading increases until finally reaching a plateau of $j \approx 6$ mA cm⁻² at CoPc loadings of ~4 x 10⁻⁹ mol cm⁻². The fact that these CoPc-P4VP/GP/GCE films with high GP loading plateau in activity, rather than decrease, at high CoPc loading and film thickness suggest that charge transport may not be the main limitation to activity. Instead, we suspect that either detrimental CoPc aggregation¹⁸ due to high CoPc loading or poor CO₂ and H⁺ transport to interior sites due to the increased film thickness may limit activity at high CoPc loadings in the high-GP films. Note that the same plateauing effect is seen for the CoPc-P4VP/EPG system in Figure 2a.

As previously discussed, for CoPc-P4VP/GP/GCE films with moderate GP loadings of ≤ 0.26 mg cm⁻², there is a decrease in measured activity with increasing CoPc loading (Figure 3a). We postulate that this decrease in activity at higher CoPc loading is due to further spacing between the GP particles in the film as the CoPc loading and film thickness increase, which in turn leads to inefficient charge transport and decreased activity compared to the thinner films at the same GP

loading and decreased CoPc loadings. To test this postulate, we designed a set of experiments keeping the GP:CoPc-P4VP ratios constant. Three catalyst preparation suspensions were prepared where the amounts of CoPc (0.0125 mM) and P4VP (0.75% w/v) were the same in each suspension, but the amount of GP differed (1 mg/mL, 5 mg/mL, 10 mg/mL). The suspensions were then centrifuged, the supernatant decanted, and the resultant deposition inks were deposited onto the GCEs according to the procedure in the Experimental section. Sequential layers of the deposition inks were then added to the surface to increase simultaneously the CoPc, P4VP, and GP loading while keeping the ratio of the three loadings constant. The resulting specific film compositions are reported in Supplementary Table S8-S13. In each case, the activity increases with increasing CoPc loading to a plateau at CoPc loadings of ~1.25 x 10⁻⁹ mol cm⁻² as shown in Figure 4 and reported in Supplementary Tables S25-S27.

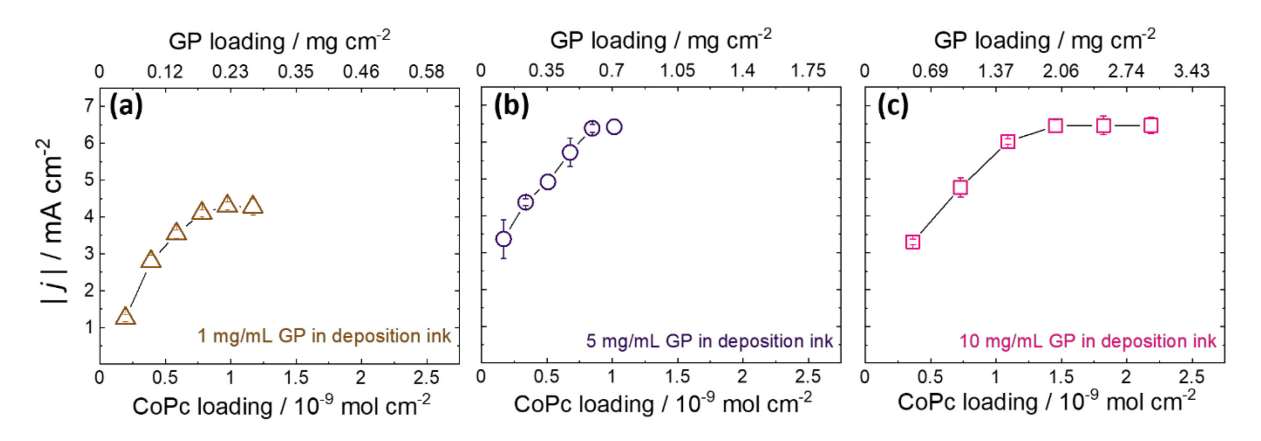


Figure 4. A plot of the absolute value of the average total measured current density from RDE-CA measurements at -1.25 V vs SCE in CO₂-saturated 0.1 M phosphate solution at pH 5 reported as a function of CoPc loading for CoPc-P4VP/GP/GCE. The GP:CoPc-P4VP ratio is constant within each prepared set of catalyst preparation suspensions: 0.0125 mM CoPc with 0.75% P4VP and either (a) 1 mg/mL, (b) 5 mg/mL, or (c) 10 mg/mL of graphite powder. Note that even though the CoPc and P4VP loadings in the preparation suspensions were the same for each GP loading, the loadings are different in the deposition ink after the centrifugation step, and are summarized in Supplementary Tables S9, S11, and S13. The CoPc, P4VP, and GP loadings were increased by adding additional layers of the deposition ink in 10 µL increments, and so the CoPc:P4VP:GP ratio remained constant in each set of experiments. The film thickness increased along with the CoPc loading due to the stepwise deposition of P4VP and GP. All data points are reported as averages from at least three experiments on independently prepared samples, and the error bars represent standard deviations. The solid black lines connecting the points are guides to the eye, and not indicative of fits of the data. For all measurements, the loading of CoPc, P4VP, and GP for each data point is summarized in Supplementary Tables S8-S13, representative RDE-CAs for selected CoPc loadings are shown in Supplementary Figure S9-S11, and activity data is summarized in Supplementary Tables S25-S27.

The fact that the activity plateaus as the film loading increases when the GP:CoPc-P4VP ratio remains constant in Figure 4 suggests that charge transport is not limiting even at high film

loadings. In contrast, for CoPc-P4VP/GP/GCE films with fixed moderate GP loadings of ≤ 0.26 mg cm⁻² in Figure 3, the GP:CoPc-P4VP ratio decreases as the film loading increases, resulting in decreased activity. The different activity trends for these two systems supports our postulate that the decreased activity for CoPc-P4VP/GP/GCE films at high film loading and low GP loading is due to inefficient charge transport due to the increased spacing between the GP particles, and that this limitation can be overcome by keeping the CoPc:P4VP:GP ratios constant, thereby ensuring that GP loading increases at the same rate as CoPc and P4VP. The plateau in activity at sufficiently high GP and CoPc-P4VP loadings in Figure 4a, b, and c is qualitatively similar to the plateau in activity observed for the CoPc-P4VP/GP/GCE films at high fixed GP loadings ≥ 0.51 mg cm⁻² in Figure 3a. In particular, the plateau in activity occurs at similar CoPc and P4VP loading in Figures 4b and 4c, even though the GP loading is lower at this CoPc and P4VP concentration in Figure 4b compared to that in Figure 4c. These results suggest that as long as the GP:CoPc:P4VP ratio is sufficiently large and remains constant during film deposition, then charge transport is not rate limiting regardless of the film loading and thickness. Instead, the activity in systems with sufficiently large GP:CoPc:P4VP ratios may be limited by decreased H⁺ or CO₂ transport to interior CoPc sites within the film, or by CoPc aggregation at higher loadings that may limit the number of active CoPc sites.

One component contributing to the high activity and selectivity of the CoPc-P4VP/EPG system is the axial coordination of the pyridyl moieties on the polymer to the CoPc center. 13,24,36 This axial coordination of σ -donating moieties to CoPc shifts the rate-determining step of the CO₂ reduction mechanism from an initial CO₂ binding step to a subsequent proton transfer event, resulting in increases in selectivity and activity for the CO₂RR compared to four-coordinate CoPc systems. 24,44 An important question is whether such axial-coordination is still beneficial to the

activity of CoPc-P4VP/GP/GCE systems. In our systems with added GP, strong interaction between the CoPc and the GP particles are likely necessary to facilitate efficient charge transport, ^{33,57,61,62} and these CoPc-GP interactions might be inhibited by axial coordination of the CoPc to the polymer or other pyridyl species. To help address this question, we measured the activity and selectivity of the CO₂RR as we modulated the extent of axial coordination through systematic modifications of the CoPc-polymer-GP system. In particular, we compared the CO₂RR performance of 1) CoPc-P4VP/GP/GCE, where CoPc is axially coordinated to the pyridyl moieties in P4VP;^{24,36} 2) CoPc-P2VP/GP/GCE, where no axial coordination between CoPc and the poly-2-vinylpyridine (P2VP) polymer is expected;^{24,36} 3) CoPc(pyNMe₂)-P2VP/GP/GCE, where the CoPc is axially coordinated to the strong σ-donor 4-dimethylaminopyridine (pyNMe₂) and embedded in the non-coordinating (P2VP) polymer,⁴⁴ and 4) CoPc-P4CS/GP/GCE, where we expect sluggish activity due to both a lack of axial coordination to the poly-4-chloropolystyrene polymer (P4CS) and poor H⁺ transport due to lack of multisite proton relays in the system.²⁴

The results of the measured activity at different CoPc loadings with a fixed CoPc: polymer ratio and a fixed GP loading of 0.51 mg cm⁻² are shown in Figure 5. In general, the systems with axial coordination to the pyridyl moieties on the P4VP polymer (CoPc-P4VP/GP/GCE) or prepared as the 5-coordinate CoPc(pyNMe₂) species and encapsulated in the non-coordinating P2VP polymer (CoPc(pyNMe₂)-P2VP/GP/GCE) showed similar high activity at most CoPc loadings. Both CoPc-P4VP/GP/GCE and CoPc(pyNMe₂)-P2VP/GP/GCE showed slightly higher activity than CoPc-P2VP/GP/GCE with no axial coordination at most CoPc loadings > 1 × 10⁻⁹ mol cm⁻², but the difference was not as pronounced as when comparing similar systems deposited on EPG. For instance, we had previously shown that CoPc-P4VP/EPG operates with > 4× the activity of CoPc-P2VP/EPG, ^{13,24} whereas CoPc-P4VP/GP/GCE operates with only ~1.5× the

activity of CoPc-P2VP/GP/GCE at most CoPc loadings (Figure 5). These results suggest that axial coordination is still important to maximizing activity of the system with added GP, but it has a smaller effect on the overall activity compared to systems without added GP. One explanation may be that the CoPc partially coordinates to heteroatoms on the GP particles, meaning that some fraction of CoPc in the non-coordinating P2VP case is still 5-coordinate. Such partial axial coordination of CoPc to surface species carbon systems has been previously suggested,²⁷ and could result in the observed higher-than-expected activity for CoPc-P2VP/GP/GCE.

Note that in all systems in Figure 5, there is a decrease in activity at the highest CoPc loadings measured. In particular, in the case of CoPc(pyNMe₂)-P2VP/GP/GCE there is a measureable decrease in activity at the highest CoPc loading, to the point where the activity of CoPc(pyNMe₂)-P2VP/GP/GCE and CoPc-P2VP/GP/GCE have similar activities at the highest CoPc loading. We attribute this decreased activity at the highest CoPc loadings to the inefficient charge transport. In the systems reported in Figure 5, GP loading is held constant as the film loading increases. As we discussed above for films with intermediate GP loadings in Figure 3, as the film loading increases, the individual GP particles are spaced further apart, and charge transport is inhibited at higher film loadings. The important takeaway from these studies is that axial coordination increases activity for the CO₂RR by the CoPc system with added GP, but this axial coordination becomes less important under charge transport limitations. Even when we encapsulate CoPc(pyNMe₂) within the coordinating P4VP polymer, to ensure CoPc is axially coordinated, the activity at the highest CoPc loading is similar to that for CoPc-P2VP/GP/GCE (see Supplementary Table S18). CoPc aggregation and/or inefficient CO2 or H+ transport at higher CoPc and film loadings may also contribute to this observed decreased activity.

We also measured the activity in CoPc-P4CS/GP/GCE, where the polymer is unable to coordinate axially to the CoPc, and the polymer cannot participate in the proton transfer mechanism via multisite proton relays. In previous studies, we used PS as a non-coordinating, inert polymer.²⁴ Unfortunately, the large polymer loadings used in the preparation suspensions in this study resulted in aggregation and precipitation of the PS from the suspensions. P4CS was chosen as an alternate polymer that does not aggregate under these conditions due the added steric bulk of the Cl group, but also does not interact with the CoPc and does not have a proton-shuttling moiety. The electrochemical stability of P4CS has not been rigorously addressed in the literature, but it shows similar stability to thermal degradation compared to PS and P4VP,⁶³⁻⁶⁵ and we observed no evidence of activity loss or polymer degradation during our electrochemical measurements. We expected that CoPc-P4CS should behave similarly to CoPc-PS with low activity for the CO₂RR. Indeed, CoPc-P4CS/GP/GCE showed little activity for the CO₂RR as expected. In previous studies, we used CoPc-polystyrene (CoPc-PS) to show that the pyridyl moieties within the polymer are vital to the effects that we see due to P4VP encapsulation of CoPc.

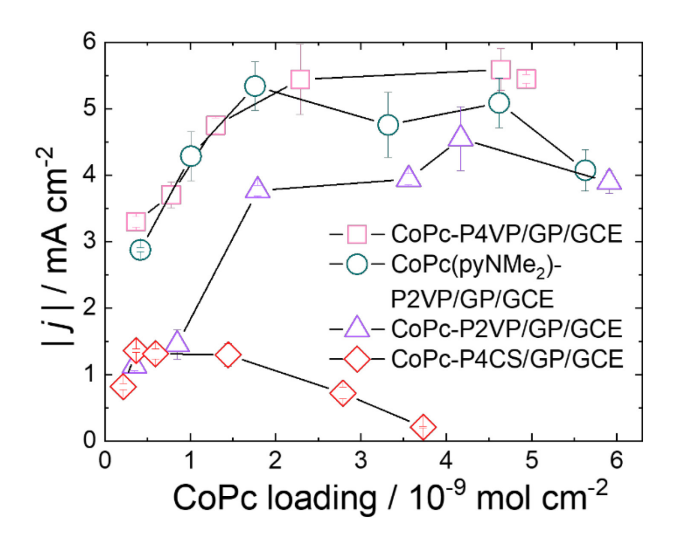


Figure 5. The effect of axial coordination on activity of catalyst-polymer composites with graphite powder (GP) on GCEs. The overall activity of the system is higher when the CoPc is coordinated to either the polymer (in the case of CoPc-P4VP/GP/GCE) or to a fifth ligand (in the case CoPc(pyNMe₂)-P2VP/GP/GCE). Activity is reported as the absolute value of the average total measured current density from RDE-CA measurements at –1.25 V vs SCE in CO₂-saturated 0.1 M phosphate solution at pH 5 reported as a function of CoPc loading. For each set of measurements, the GP loading is 10 mg/mL or 0.51 mg/cm² and the CoPc:polymer ratio stays constant as the CoPc loading increases. All data points are reported as averages from at least three experiments on independently prepared samples, and the error bars represent standard deviations. The solid black lines connecting the points are guides to the eye, and not indicative of fits of the data. For all measurements, the loading of CoPc, polymer, and GP for each data point is summarized in Supplementary Tables S2 and S14-S16, representative RDE-CAs for selected CoPc loadings are shown in Supplementary Figures S2 and S12-S14, and activity data is summarized in Supplementary Tables S21 and S28-S30.

Based on the measurements above, we chose an optimized loading for CoPc-P4VP/GP/GCE consisting of 0.05 mM CoPc -3% P4VP -1% GP in the preparation slurry, corresponding to 0.023 mM CoPc -0.3% P4VP -1% GP deposition ink and we conducted selectivity measurements

for the CO₂RR at this optimized loading. We compared the selectivity measurements for CoPc-P4VP/GP/GCE to those for CoPc-P2VP/GP/GCE and CoPc(pyNMe₂)-P2VP/GP/GCE at similar CoPc, polymer, and CP loadings as shown in Figure 6. The trends in selectivity for the CoPcpolymer/GP/GCE systems are qualitatively similar to those observed on the CoPc-polymer/EPG systems without the added GP. ^{13,24} In particular, on both EPG and GP/GCE, CoPc-P4VP and CoPc(pyNMe₂)-P2VP show the highest selectivity for the CO₂RR due to the synergistic effects of axial coordination facilitating CO₂ binding and the polymer controlling H⁺ transport and inhibiting the competitive HER. In comparison, on both EPG and GP/GCE, CoPc-P2VP shows slightly lower selectivity for the CO₂RR—it benefits from the controlled H⁺ transport, but not the axial coordination effects. The systems on GP/GCE overall have slightly lower selectivity for the CO₂RR compared to the systems on EPG, and we attribute this to increased background HER on the GP itself. Control experiments conducted with CoPc-P4VP/GP prepared at the same polymer and CoPc loadings but without centrifugation showed similar Faradaic Efficiency for CO production of 82% compared to the centrifuged CoPc-P4VP/GP/GCE case (Table S31), but substantially lower overall activity in the CPE measurements consistent with our RDE-CA measurements of the same system (Figure S1).

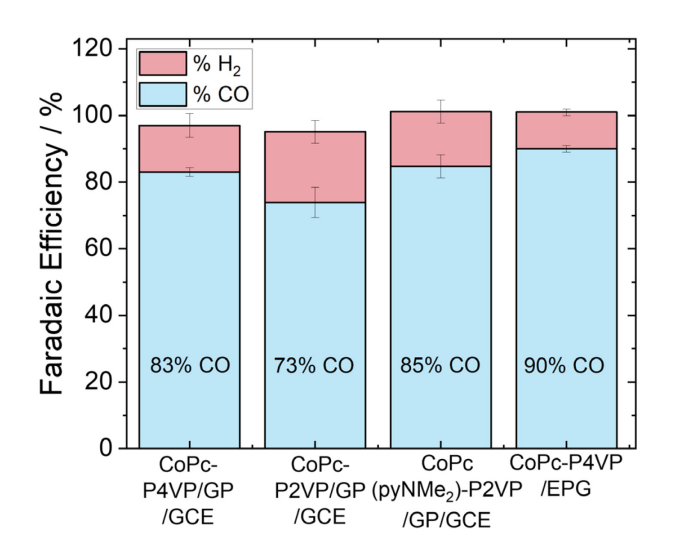


Figure 6. The measured Faradaic Efficiency for different CoPc-polymer systems on GP/GCE and EPG. CoPc-P4VP and CoPc(pyNMe₂)-P2VP operate with the highest Faradaic Efficiency, and thus the highest selectivity for the CO₂RR, on GP/GCE and EPG. CoPc-P2VP operates with comparatively lower CO₂RR selectivity. The CoPc-P4VP system on GP/GCE operates with similar but slightly lower Faradaic Efficiency than of that on EPG, and this is attributed to the higher background HER on the added GP in the GP/GCE system. All reported Faradaic efficiencies are reported as averages from at least three CPE experiments on independently prepared samples, and the error bars represent standard deviations. The loading of CoPc, polymer, and GP for each data point is summarized in Supplementary Table S19, representative current-potential traces for each CPE are shown in Supplementary Figures S15-S18, and the metrics from the CPE measurements are summarized in Supplementary Table S31.

CONCLUSIONS

Incorporating graphite powder into a catalyst-polymer composite system such as CoPc-P4VP increases charge transport and therefore increases activity—this is expected activity based on numerous previous studies. Importantly, we developed a specific multistep deposition procedure that maximizes the interactions between the CoPc and GP to facilitate efficient charge transport.

We show that there is a point of diminishing returns where further increasing the graphite powder loading, where sufficient loading of either 0.51 mg cm⁻² or 0.76 mg cm⁻² resulted in similar overall activity (Figure 3a). At low to moderate constant GP loadings, increasing the CoPc and P4VP polymer loadings results in losses in activity at sufficiently high film thicknesses, presumably due to inefficient charge transport (Figure 3a).

When GP loading remains constant in relation to CoPc and P4VP, increasing the CoPc and P4VP polymer loadings results in a plateau, not a loss, in activity at sufficiently high catalyst loading (Figure 4). This plateau in the catalytic activity at high CoPc, P4VP, and GP loadings is attributed to either inefficient H⁺ and CO₂ transport to interior CoPc sites, or lower per-Co activity due to CoPc aggregation since the GP:CoPc:P4VP ratio remained constant, and was therefore sufficiently large to allow for charge transport as the film thickness increased. Axial coordination is still required for the highest activity in the polymer composite systems even in the presence of GP (Figure 5), suggesting that the CoPc does not fully coordinate to heteroatoms on the GP surface, although some extent of coordination between CoPc and the GP surface may be present.

Based on the various activity measurements as a function of CoPc, P4VP, and GP loading, we determined a set of optimized loading conditions that maximized the catalytic activity. Under these optimized conditions, we showed that the selectivity for the CO₂RR over competitive HER was similar to those measured previously on EPG, but with much higher catalytic activity in the GP/GCE case (Figure 6). The detailed study presented here will be used in future studies to develop optimal loading conditions for other polymer-catalyst composite systems with various carbon supports. Future studies for this system may also include *in situ* XAS measurements to understand better the nature of the catalyst/polymer/GP interactions as a function of loading and applied potential.

ACKNOWLEDGMENTS

We thank Qi Wang and Samuel Michaud for useful discussions regarding experimental design and product quantification. We also thank William Dean and Weixuan Nie for helping collect SEM images. ICP-MS measurements were conducted with support from the University of Michigan, with special thanks to James Windak for assistance with the ICP-MS measurements. The authors acknowledge the University of Michigan College of Engineering for financial support and the Michigan Center for Materials Characterization for use of the SEM and staff assistance. This work was supported by an NSF-CAREER grant (CHE-1751791) and a Cottrell Scholar award, a program of the Research Corporation for Science Advancement. T. L. S. was partially supported by the National Science Foundation Graduate Research Fellowship Program (DGE 1256260) and a University of Michigan Rackham Merit Fellowship. Y.L. was partially supported by a Rackham One-Term Dissertation Fellowship from the University of Michigan. J.B.E. was partially supported by a Walter Yates Award from the University of Michigan.

ASSOCIATED CONTENT

Supporting Information. Supporting Information is available free of charge on the ACS website. Publications website at DOI: 10.1021/XXX.

Additional details regarding catalyst and polymer loading and preparation conditions,
 tables with activity measurements, faradaic efficiency results, representative RDE-CAs,
 and comparison between centrifuged and non-centrifuged CoPc-P4VP/GP/GCE systems.

AUTHOR INFORMATION

Corresponding Author

*Email for C. C. L. M.: cmccrory@umich.edu

Author Contributions

The manuscript was written through contributions of all authors. All authors have given approval to the final version of the manuscript. #T.L.S. and Y.L. contributed equally to this work.

ORCID

Taylor L. Soucy: <u>0000-0002-0090-6721</u>

Yingshuo Liu: <u>0000-0003-4780-8384</u>

Jonah B. Eisenberg: <u>0000-0003-3581-6926</u>

Charles C. L. McCrory: <u>0000-0001-9039-7192</u>

REFERENCES

- (1) Meshitsuka, S.; Ichikawa, M.; Tamaru, K. "Electrocatalysis by metal phthalocyanines in the reduction of carbon dioxide," *J. Chem. Soc., Chem. Commun.* **1974**, 158-159. http://dx.doi.org/10.1039/C39740000158
- (2) Lieber, C. M.; Lewis, N. S. "Catalytic reduction of carbon dioxide at carbon electrodes modified with cobalt phthalocyanine," *J. Am. Chem. Soc.* **1984**, *106*, 5033-5034. http://dx.doi.org/10.1021/ja00329a082
- (3) Yoshida, T.; Kamato, K.; Tsukamoto, M.; Iida, T.; Schlettwein, D.; Wöhrle, D.; Kaneko, M. "Selective electroacatalysis for CO₂ reduction in the aqueous phase using cobalt phthalocyanine/poly-4-vinylpyridine modified electrodes," *J. Electroanal. Chem.* **1995**, *385*, 209-225. http://dx.doi.org/10.1016/0022-0728(94)03762-R
- (4) Nyokong, T. "Equilibrium and kinetic studies of the reaction between pyridine and cobalt(II) phthalocyanine in DMSO," *Polyhedron* **1995**, *14*, 2325-2329. http://dx.doi.org/https://doi.org/10.1016/0277-5387(95)00090-F
- (5) Abe, T.; Yoshida, T.; Tokita, S.; Taguchi, F.; Imaya, H.; Kaneko, M. "Factors affecting selective electrocatalytic CO₂ reduction with cobalt phthalocyanine incorporated in a polyvinylpyridine membrane coated on a graphite electrode," *J. Electroanal. Chem.* **1996**, *412*, 125-132. http://dx.doi.org/10.1016/0022-0728(96)04631-1
- (6) Abe, T.; Imaya, H.; Yoshida, T.; Tokita, S.; Schlettwein, D.; Wöhrle, D.; Kaneko, M. "Electrochemical CO2 Reduction Catalysed by Cobalt Octacyanophthalocyanine and its

Mechanism," *J. Porphyrins Phthalocyanines* **1997**, *01*, 315-321. http://dx.doi.org/10.1002/(sici)1099-1409(199710)1:4<315::Aid-jpp35>3.0.Co;2-v

- (7) Schulte, K.; Swarbrick, J. C.; Smith, N. A.; Bondino, F.; Magnano, E.; Khlobystov, A. N. "Assembly of Cobalt Phthalocyanine Stacks inside Carbon Nanotubes," *Adv. Mater.* **2007**, *19*, 3312-3316. http://dx.doi.org/https://doi.org/10.1002/adma.200700188
- (8) Wang, Y.; Hu, N.; Zhou, Z.; Xu, D.; Wang, Z.; Yang, Z.; Wei, H.; Kong, E. S.-W.; Zhang, Y. "Single-walled carbon nanotube/cobalt phthalocyanine derivative hybrid material: preparation, characterization and its gas sensing properties," *J. Mater. Chem.* **2011**, *21*, 3779-3787. http://dx.doi.org/10.1039/C0JM03567J
- (9) Zhao, H.; Zhang, Y.; Zhao, B.; Chang, Y.; Li, Z. "Electrochemical Reduction of Carbon Dioxide in an MFC–MEC System with a Layer-by-Layer Self-Assembly Carbon Nanotube/Cobalt Phthalocyanine Modified Electrode," *Environ. Sci. Technol.* **2012**, *46*, 5198-5204. http://dx.doi.org/10.1021/es300186f
- (10) Hosu, I. S.; Wang, Q.; Vasilescu, A.; Peteu, S. F.; Raditoiu, V.; Railian, S.; Zaitsev, V.; Turcheniuk, K.; Wang, Q.; Li, M.; Boukherroub, R.; Szunerits, S. "Cobalt phthalocyanine tetracarboxylic acid modified reduced graphene oxide: a sensitive matrix for the electrocatalytic detection of peroxynitrite and hydrogen peroxide," *RSC Advances* **2015**, *5*, 1474-1484. http://dx.doi.org/10.1039/C4RA09781E
- (11) Li, N.; Lu, W.; Pei, K.; Chen, W. "Interfacial peroxidase-like catalytic activity of surface-immobilized cobalt phthalocyanine on multiwall carbon nanotubes," *RSC Advances* **2015**, *5*, 9374-9380. http://dx.doi.org/10.1039/C4RA15306E

- (12) Manbeck, G. F.; Fujita, E. "A review of iron and cobalt porphyrins, phthalocyanines and related complexes for electrochemical and photochemical reduction of carbon dioxide," *J. Porphyrins Phthalocyanines* **2015**, *19*, 45-64. http://dx.doi.org/10.1142/S1088424615300013
- (13) Kramer, W. W.; McCrory, C. C. L. "Polymer coordination promotes selective CO₂ reduction by cobalt phthalocyanine," *Chem. Sci.* **2016**, *7*, 2506-2515. http://dx.doi.org/10.1039/C5SC04015A
- (14) Han, N.; Wang, Y.; Ma, L.; Wen, J.; Li, J.; Zheng, H.; Nie, K.; Wang, X.; Zhao, F.; Li, Y.; Fan, J.; Zhong, J.; Wu, T.; Miller, D. J.; Lu, J.; Lee, S.-T.; Li, Y. "Supported Cobalt Polyphthalocyanine for High-Performance Electrocatalytic CO₂ Reduction," *Chem* **2017**, *3*, 652-664. http://dx.doi.org/10.1016/j.chempr.2017.08.002
- (15) Zhang, X.; Wu, Z.; Zhang, X.; Li, L.; Li, Y.; Xu, H.; Li, X.; Yu, X.; Zhang, Z.; Liang, Y.; Wang, H. "Highly selective and active CO2 reduction electrocatalysts based on cobalt phthalocyanine/carbon nanotube hybrid structures," *Nat. Commun.* **2017**, *8*, 14675. http://dx.doi.org/10.1038/ncomms14675
- (16) Li, N.; Wang, Y.; Wu, C.; Lu, W.; Pei, K.; Chen, W. "Bioinspired catalytic generation of high-valent cobalt-oxo species by the axially coordinated CoPc on pyridine-functionalized MWCNTs for the elimination of organic contaminants," *Appl. Surf. Sci.* **2018**, *434*, 1112-1121. http://dx.doi.org/10.1016/j.apsusc.2017.11.048
- (17) Wu, H.; Zeng, M.; Zhu, X.; Tian, C.; Mei, B.; Song, Y.; Du, X.-L.; Jiang, Z.; He, L.; Xia, C.; Dai, S. "Defect Engineering in Polymeric Cobalt Phthalocyanine Networks for Enhanced

Electrochemical CO2 Reduction," *ChemElectroChem* **2018**, *5*, 2717-2721. http://dx.doi.org/10.1002/celc.201800806

- (18) Zhu, M.; Ye, R.; Jin, K.; Lazouski, N.; Manthiram, K. "Elucidating the Reactivity and Mechanism of CO₂ Electroreduction at Highly Dispersed Cobalt Phthalocyanine," *ACS Energy Lett.* **2018**, *3*, 1381-1386. http://dx.doi.org/10.1021/acsenergylett.8b00519
- (19) Boutin, E.; Wang, M.; Lin, J. C.; Mesnage, M.; Mendoza, D.; Lassalle-Kaiser, B.; Hahn, C.; Jaramillo, T. F.; Robert, M. "Aqueous Electrochemical Reduction of Carbon Dioxide and Carbon Monoxide into Methanol with Cobalt Phthalocyanine," *Angew. Chem. Int. Ed.* **2019**, *58*, 16172-16176. http://dx.doi.org/10.1002/anie.201909257
- (20) Chen, J.; Li, J.; Liu, W.; Ma, X.; Xu, J.; Zhu, M.; Han, Y.-F. "Facile synthesis of polymerized cobalt phthalocyanines for highly efficient CO2 reduction," *Green Chem.* **2019**, *21*, 6056-6061. http://dx.doi.org/10.1039/C9GC02705J
- (21) Choi, J.; Wagner, P.; Gambhir, S.; Jalili, R.; MacFarlane, D. R.; Wallace, G. G.; Officer, D. L. "Steric Modification of a Cobalt Phthalocyanine/Graphene Catalyst To Give Enhanced and Stable Electrochemical CO2 Reduction to CO," *ACS Energy Lett.* **2019**, *4*, 666-672. http://dx.doi.org/10.1021/acsenergylett.8b02355
- (22) Corbin, N.; Zeng, J.; Williams, K.; Manthiram, K. "Heterogeneous molecular catalysts for electrocatalytic CO2 reduction," *Nano Research* **2019**, *12*, 2093-2125. http://dx.doi.org/10.1007/s12274-019-2403-y
- (23) Lin, L.; Li, H.; Yan, C.; Li, H.; Si, R.; Li, M.; Xiao, J.; Wang, G.; Bao, X. "Synergistic Catalysis over Iron-Nitrogen Sites Anchored with Cobalt Phthalocyanine for Efficient CO2

Electroreduction," *Adv. Mater.* **2019**, *31*, 1903470. http://dx.doi.org/https://doi.org/10.1002/adma.201903470

- (24) Liu, Y.; McCrory, C. C. L. "Modulating the mechanism of electrocatalytic CO₂ reduction by cobalt phthalocyanine through polymer coordination and encapsulation," *Nat. Commun.* **2019**, 10, 1683. http://dx.doi.org/10.1038/s41467-019-09626-8
- (25) Ren, S.; Joulié, D.; Salvatore, D.; Torbensen, K.; Wang, M.; Robert, M.; Berlinguette, C. P. "Molecular electrocatalysts can mediate fast, selective CO2 reduction in a flow cell," *Science* **2019**, *365*, 367-369. http://dx.doi.org/10.1126/science.aax4608
- (26) Roy, S.; Reisner, E. "Visible-Light-Driven CO₂ Reduction by Mesoporous Carbon Nitride Modified with Polymeric Cobalt Phthalocyanine," *Angew. Chem. Int. Ed.* **2019**, *58*, 12180-12184. http://dx.doi.org/10.1002/anie.201907082
- (27) Wang, J.; Huang, X.; Xi, S.; Lee, J.-M.; Wang, C.; Du, Y.; Wang, X. "Linkage Effect in the Heterogenization of Cobalt Complexes by Doped Graphene for Electrocatalytic CO2 Reduction," *Angew. Chem. Int. Ed.* **2019**, *58*, 13532-13539. http://dx.doi.org/10.1002/anie.201906475
- (28) Wang, M.; Torbensen, K.; Salvatore, D.; Ren, S.; Joulié, D.; Dumoulin, F.; Mendoza, D.; Lassalle-Kaiser, B.; Işci, U.; Berlinguette, C. P.; Robert, M. "CO₂ electrochemical catalytic reduction with a highly active cobalt phthalocyanine," *Nat. Commun.* **2019**, *10*, 3602. http://dx.doi.org/10.1038/s41467-019-11542-w

- (29) Wu, Y.; Jiang, Z.; Lu, X.; Liang, Y.; Wang, H. "Domino electroreduction of CO₂ to methanol on a molecular catalyst," *Nature* **2019**, *575*, 639-642.

 http://dx.doi.org/10.1038/s41586-019-1760-8
- (30) Zhu, M.; Chen, J.; Guo, R.; Xu, J.; Fang, X.; Han, Y.-F. "Cobalt phthalocyanine coordinated to pyridine-functionalized carbon nanotubes with enhanced CO2 electroreduction," *Applied Catalysis B: Environmental* **2019**, *251*, 112-118. http://dx.doi.org/10.1016/j.apcatb.2019.03.047
- (31) Chen, J.; Zhu, M.; Li, J.; Xu, J.; Han, Y.-F. "Structure–Activity Relationship of the Polymerized Cobalt Phthalocyanines for Electrocatalytic Carbon Dioxide Reduction," *J. Phys. Chem. C* **2020**, *124*, 16501-16507. http://dx.doi.org/10.1021/acs.jpcc.0c04741
- (32) De Riccardis, A.; Lee, M.; Kazantsev, R. V.; Garza, A. J.; Zeng, G.; Larson, D. M.; Clark, E. L.; Lobaccaro, P.; Burroughs, P. W. W.; Bloise, E.; Ager, J. W.; Bell, A. T.; Head-Gordon, M.; Mele, G.; Toma, F. M. "Heterogenized Pyridine-Substituted Cobalt(II) Phthalocyanine Yields Reduction of CO2 by Tuning the Electron Affinity of the Co Center," *ACS Appl. Mater. Interfaces* **2020**, *12*, 5251-5258. http://dx.doi.org/10.1021/acsami.9b18924
- (33) Huai, M.; Yin, Z.; Wei, F.; Wang, G.; Xiao, L.; Lu, J.; Zhuang, L. "Electrochemical CO₂ reduction on heterogeneous cobalt phthalocyanine catalysts with different carbon supports," *Chem. Phys. Lett.* **2020**, *754*, 137655. http://dx.doi.org/10.1016/j.cplett.2020.137655
- (34) Li, T.-T.; Mei, Y.; Li, H.; Qian, J.; Wu, M.; Zheng, Y.-Q. "Highly Selective and Active Electrochemical Reduction of CO2 to CO on a Polymeric Co(II) Phthalocyanine@Graphitic

Carbon Nitride Nanosheet–Carbon Nanotube Composite," *Inorg. Chem.* **2020**. http://dx.doi.org/10.1021/acs.inorgchem.0c01977

- (35) Lin, L.; Liu, T.; Xiao, J.; Li, H.; Wei, P.; Gao, D.; Nan, B.; Si, R.; Wang, G.; Bao, X. "Enhancing CO2 Electroreduction to Methane with a Cobalt Phthalocyanine and Zinc–Nitrogen–Carbon Tandem Catalyst," *Angew. Chem. Int. Ed.* **2020**, *59*, 22408-22413. http://dx.doi.org/https://doi.org/10.1002/anie.202009191
- (36) Liu, Y.; Deb, A.; Leung, K. Y.; Nie, W.; Dean, W. S.; Penner-Hahn, J. E.; McCrory, C. C. L. "Determining the coordination environment and electronic structure of polymer-encapsulated cobalt phthalocyanine under electrocatalytic CO₂ reduction conditions using in situ X-Ray absorption spectroscopy," *Dalton Trans.* **2020**, *49*, 16329-16339.

 http://dx.doi.org/10.1039/D0DT01288B
- (37) Xia, Y.; Kashtanov, S.; Yu, P.; Chang, L.-Y.; Feng, K.; Zhong, J.; Guo, J.; Sun, X. "Identification of dual-active sites in cobalt phthalocyanine for electrochemical carbon dioxide reduction," *Nano Energy* **2020**, *67*, 104163. http://dx.doi.org/10.1016/j.nanoen.2019.104163
- (38) Wang, X.; Cai, Z.-F.; Wang, Y.-Q.; Feng, Y.-C.; Yan, H.-J.; Wang, D.; Wan, L.-J. "In Situ Scanning Tunneling Microscopy of Cobalt-Phthalocyanine-Catalyzed CO2 Reduction Reaction," *Angew. Chem. Int. Ed.* **2020**, *59*, 16098-16103. http://dx.doi.org/10.1002/anie.202005242
- (39) Wu, Y.; Hu, G.; Rooney, C. L.; Brudvig, G. W.; Wang, H. "Heterogeneous Nature of Electrocatalytic CO/CO2 Reduction by Cobalt Phthalocyanines," *ChemSusChem* **2020**, *n/a*. http://dx.doi.org/10.1002/cssc.202001396

- (40) Yang, Z.; Zhang, X.; Long, C.; Yan, S.; Shi, Y.; Han, J.; Zhang, J.; An, P.; Chang, L.; Tang, Z. "Covalently anchoring cobalt phthalocyanine on zeolitic imidazolate frameworks for efficient carbon dioxide electroreduction," *CrystEngComm* **2020**, *22*, 1619-1624. http://dx.doi.org/10.1039/C9CE01517E
- (41) Zeng, J. S.; Corbin, N.; Williams, K.; Manthiram, K. "Kinetic Analysis on the Role of Bicarbonate in Carbon Dioxide Electroreduction at Immobilized Cobalt Phthalocyanine," *ACS Catal.* **2020**, *10*, 4326-4336. http://dx.doi.org/10.1021/acscatal.9b05272
- (42) Zhang, H.; Min, S.; Wang, F.; Zhang, Z. "Immobilizing cobalt phthalocyanine into a porous carbonized wood membrane as a self-supported heterogenous electrode for selective and stable CO2 electroreduction in water," *Dalton Trans.* **2020**, *49*, 15607-15611. http://dx.doi.org/10.1039/D0DT03304A
- (43) Gu, S.; Marianov, A. N.; Zhu, Y.; Jiang, Y. "Cobalt porphyrin immobilized on the TiO2 nanotube electrode for CO2 electroreduction in aqueous solution," *J. Energy Chem.* **2021**, *55*, 219-227. http://dx.doi.org/https://doi.org/10.1016/j.jechem.2020.06.067
- (44) Rivera Cruz, K. E.; Liu, Y.; Soucy, T. L.; Zimmerman, P. M.; McCrory, C. C. L. "Increasing the CO2 Reduction Activity of Cobalt Phthalocyanine by Modulating the σ-Donor Strength of Axially Coordinating Ligands," *ACS Catalysis* **2021**, 13203-13216. http://dx.doi.org/10.1021/acscatal.1c02379
- (45) Sun, L.; Reddu, V.; Fisher, A. C.; Wang, X. "Electrocatalytic reduction of carbon dioxide: opportunities with heterogeneous molecular catalysts," *Energy Environ. Sci.* **2020**, *13*, 374-403. http://dx.doi.org/10.1039/C9EE03660A

- (46) Yamanaka, I.; Tabata, K.; Mino, W.; Furusawa, T. "Electroreduction of carbon dioxide to carbon monoxide by Co-pthalocyanine electrocatalyst under ambient conditions," *ISIJ International* **2015**, *55*, 399-403.
- (47) Liu, Y.; Leung, K. Y.; Michaud, S. E.; Soucy, T. L.; McCrory, C. C. L. "Controlled Substrate Transport To Electrocatalyst Active Sites For Enhanced Selectivity In The Carbon Dioxide Reduction Reaction," *Comments Inorg. Chem.* **2019**, 1-28. http://dx.doi.org/10.1080/02603594.2019.1628025
- (48) Zhu, M.; Chen, J.; Huang, L.; Ye, R.; Xu, J.; Han, Y.-F. "Covalently Grafting Cobalt Porphyrin onto Carbon Nanotubes for Efficient CO2 Electroreduction," *Angew. Chem. Int. Ed.* **2019**, *58*, 6595-6599. http://dx.doi.org/https://doi.org/10.1002/anie.201900499
- (49) Zhu, M.; Cao, C.; Chen, J.; Sun, Y.; Ye, R.; Xu, J.; Han, Y.-F. "Electronic Tuning of Cobalt Porphyrins Immobilized on Nitrogen-Doped Graphene for CO2 Reduction," *ACS Appl. Energy Mater.* **2019**, *2*, 2435-2440. http://dx.doi.org/10.1021/acsaem.9b00368
- (50) Bottari, G.; de la Torre, G.; Guldi, D. M.; Torres, T. "Covalent and Noncovalent Phthalocyanine–Carbon Nanostructure Systems: Synthesis, Photoinduced Electron Transfer, and Application to Molecular Photovoltaics," *Chem. Rev.* **2010**, *110*, 6768-6816. http://dx.doi.org/10.1021/cr900254z
- (51) Zhang, X.; Feng, Y.; Tang, S.; Feng, W. "Preparation of a graphene oxide–phthalocyanine hybrid through strong π–π interactions," *Carbon* **2010**, *48*, 211-216.

 http://dx.doi.org/https://doi.org/10.1016/j.carbon.2009.09.007

- (52) Wang, X.; Liu, Y.; Qiu, W.; Zhu, D. "Immobilization of tetra-tert-butylphthalocyanines on carbon nanotubes: a first step towards the development of new nanomaterials," *J. Mater. Chem.* **2002**, *12*, 1636-1639. http://dx.doi.org/10.1039/B201447E
- (53) Murakami, H.; Nakamura, G.; Nomura, T.; Miyamoto, T.; Nakashima, N. "Noncovalent porphyrin-functionalized single-walled carbon nanotubes: solubilization and spectral behaviors," *J. Porphyrins Phthalocyanines* **2007**, *11*, 418-427. http://dx.doi.org/10.1142/s1088424607000473
- (54) Tasis, D.; Tagmatarchis, N.; Bianco, A.; Prato, M. "Chemistry of Carbon Nanotubes," *Chem. Rev.* **2006**, *106*, 1105-1136. http://dx.doi.org/10.1021/cr0505690
- (55) Chen, K.; Downes, C. A.; Schneider, E.; Goodpaster, J. D.; Marinescu, S. C. "Improving and Understanding the Hydrogen Evolving Activity of a Cobalt Dithiolene Metal—Organic Framework," *ACS Appl. Mater. Interfaces* **2021**, *13*, 16384-16395.

 http://dx.doi.org/10.1021/acsami.1c01727
- (56) Bott, A. W. "Electrochemical techniques for the characterization of redox polymers," *Curr. Sep.* **2001**, *19*, 71-75.
- (57) Costentin, C.; Savéant, J.-M. "Molecular approach to catalysis of electrochemical reaction in porous films," *Curr. Opin. Electrochem.* **2019**, *15*, 58-65. http://dx.doi.org/10.1016/j.coelec.2019.03.014
- (58) Torbensen, K.; Joulié, D.; Ren, S.; Wang, M.; Salvatore, D.; Berlinguette, C. P.; Robert,
 M. "Molecular Catalysts Boost the Rate of Electrolytic CO2 Reduction," ACS Energy Lett. 2020,
 5, 1512-1518. http://dx.doi.org/10.1021/acsenergylett.0c00536

- (59) Tan, D. C. L.; Sato, H. "Enhancing Catalytic Activity of Bioanode for Glucose Biofuel Cell by Compressing Enzyme, Mediator and Carbon Support through Centrifugation," *Chem. Eur. J.* **2017**, *23*, 11485-11488. http://dx.doi.org/https://doi.org/10.1002/chem.201702100
- (60) Blanch, A. J.; Lenehan, C. E.; Quinton, J. S. "Parametric analysis of sonication and centrifugation variables for dispersion of single walled carbon nanotubes in aqueous solutions of sodium dodecylbenzene sulfonate," *Carbon* **2011**, *49*, 5213-5228.

 http://dx.doi.org/https://doi.org/10.1016/j.carbon.2011.07.039
- (61) Mak, C. H.; Han, X.; Du, M.; Kai, J.-J.; Tsang, K. F.; Jia, G.; Cheng, K.-C.; Shen, H.-H.; Hsu, H.-Y. "Heterogenization of homogeneous photocatalysts utilizing synthetic and natural support materials," *J. Mater. Chem. A* **2021**, *9*, 4454-4504.

 http://dx.doi.org/10.1039/D0TA08334H
- (62) Costentin, C.; Robert, M.; Savéant, J.-M. "Molecular catalysis of electrochemical reactions," *Curr. Opin. Electrochem.* **2017**, *2*, 26-31. http://dx.doi.org/10.1016/j.coelec.2017.02.006
- (63) Khairou, K. S.; Diab, M. A. "Stability and degradation of poly(4-vinylpyridine) and copolymers of 4-vinylpyridine with methyl methacrylate," *Polym. Degrad. Stab.* **1994**, *44*, 17-20. http://dx.doi.org/https://doi.org/10.1016/0141-3910(94)90026-4
- (64) Sikorski, R. T.; Mirkiewicz, G.; Varga, J.; Biró, O. "Influence of substituents in chloropolystyrenes and styrene copolymers on their thermal stability," *J. Therm. Anal.* **1990**, *36*, 1795-1802. http://dx.doi.org/10.1007/BF01913426

(65) Camps, M.; Jebri, A.; Drouet, J.-C. "Comparative study of thermal stabilities and limiting oxygen indexes of chlorinated, brominated, and iodinated polystyrenes," *Journal of fire sciences* **1996**, *14*, 251-262.

TOC Image

